Int. J. Electrochem. Sci., 16 **(2021)** Article Number: 211035, doi: 10.20964/2021.10.38

International Journal of
ELECTROCHEMICAL
SCIENCE
www.electrochemsci.org

N/O Co-doped Hollow Carbon Nanocapsules-Supported Ge Nanoparticles as Anodes for Excellent Performance Lithium-ion batteries

Dacheng Zhang [1,2], *Linlin Wang*[2,*], *Qian Wu*[2], *Yujie Yang*[2], *and Jingli Xu*[1,*]

[1] School of Materials Engineering, Shanghai University of Engineering Science, Shanghai 201620, P. R. China.
[2] Institute for Sustainable Energy/College of Science, Shanghai University, 99 Shangda Road, Shanghai 200444, P.R. China.
[*]E-mail: wlinlin@mail.ustc.edu.cn

Received: 15 June 2021 / *Accepted:* 10 August 2021 / *Published:* 10 September 2021

In this work, a novel N/O Co-doped hollow carbon nanocapsule-supported Ge nanoparticles nanocomposite (Ge-N/O-CNCs) was successfully prepared by a facile heating reflux method. N/O codoped hollow carbon nanocapsule-supported Ge nanoparticles not only relieve the agglomeration of Ge nanoparticles and control the volume expansion, but also facilitate the rapid transmission of electrons. In LIBs, the unique Ge-N/O-CNCs nanoarchitecture was used as the anode material. At a high current density of 1 A g^{-1}, it remains a stable specific capacity of 448 mAh g^{-1} remained after 100 cycles. Additionally, even at 3.2 A g^{-1}, this material exhibited a high-rate specific capacity of 350 mAh g^{-1}.

Keywords: Ge-N/O-CNCs, LIBs, high capacity, cycling stability

1. INTRODUCTION

Compared with commercial graphite material (372 mAh g^{-1}), germanium (Ge), with the advantage of high theoretical capacity (1623 mAh g^{-1}), has been regarded as a more worthy anode for excellent performance lithium-ion batteries (LIBs).[1-5] Nevertheless, during the lithiation/delithiation process, its disadvantages (e.g., large structural changes and serious volume expansion), [6-9] make the Ge electrode suffer capacity fading and exhibit a poor cycling lifetime, which are the main obstacles that limit Ge from becoming a commercially applicable anode material for LIBs.

One effective strategy to overcome the abovementioned problems is to reduce the microscale Ge particles to the nanoscale (such as nanoparticles [10], nanotubes [11] and nanowires [12]), which can relieve mechanical stress by reducing the distance of Li-ion diffusion and improve the electrochemical

performance of Ge. However, the aggregation effect of nanoparticles due to the reduced particle size also affects the performance of Ge anodes. Therefore, anchoring Ge directly on carbonaceous materials seems to be a more efficient strategy that can not only prohibit aggregation of the Ge nanoparticles but also cushion the volume expansion as well as improve the electrode conductivity. [13-19] For instance, Yao and Wang [14] fabricated the mesoporous Ge/C nanocomposites as anodes of LIBs. Tetraethoxygermane (TEOG), which is a source of germanium, was filled into the porous carbon matrix to prepare Ge/C nanocomposites. It shows a capacity of 736 mAh g^{-1}, as well as an excellent electrochemical performance. Furthermore, Xiao *et al.* [15] fabricated a Ge/N-doped carbon monolith as an anode for LIBs. The Ge/N-doped carbon monoliths have a continuous and conductive carbon network, in which Ge-N chemical bonds connect Ge nanoparticles to carbon, as well as a unique porous structure for suppressing the large volume change of Ge nanoparticles. It shows a specific capacity of 813 mAh g^{-1} (0.5 A g^{-1}), as well as an excellent electrochemical performance. The Li group [18] fabricated a Ge nanoparticle composite carbon nanofibre composite carbon material (Ge@CNF@C). It was prepared by anchoring Ge nanoparticles into the CNFs and then depositing a layer of carbon. The carbon nanofibres and carbon layer in the Ge@CNF@C can maintain its structural integrity during cycling and improve its cycling stability. Although the electrochemical performance of these materials has been enhanced to some extent, there is much room for designing novel Ge/C electrodes with improved electrochemical performance of Ge for LIBs with excellent performance.

Herein, we designed and synthesized a novel N/O codoped hollow carbon nanocapsule-supported Ge nanoparticles nanocomposite (Ge-N/O-CNCs) by a facile heating reflux method. [20] Ge nanoparticles are deposited in the hollow carbon nanocapsules can not only relieve the aggregation of Ge nanoparticles, but also facilitate the rapid transmission of electrons. In addition, the N/O-CNCs alleviated the volume expansion as well as improved the electrical conductivity of the Ge-N/O-CNCs electrode. Due to the unique hollow nanocapsule structure of the Ge-N/O-CNCs, the Ge-N/O-CNCs electrode shows a relatively high specific capacity with good cycle performance under a high current density. According to research, a high and reversible specific capacity of 448 mAh g^{-1} remains after 100 cycles at 1 A g^{-1} for LIBs. In addition, at 3.2 A g^{-1}, this material exhibits a high-rate specific capacity of 350 mAh g^{-1}. When returned to 0.16 A g^{-1}, its specific capacity quickly stabilized at 1011 mAh g^{-1}. Therefore, we believe that this paper optimizes the Ge-based anode material in LIBs through a simple synthesis method.

2. EXPERIMENTAL SECTION

2.1 Synthesis of Ge-N/O-CNCs.

In a typical synthesis, firstly, the N/O-CNCs (30 mg) (The N/O-CNCs were synthesized by our previous method, [20] where the micromorphology as well as composition of it were characterized by SEM, TEM, Raman spectroscopy and XPS) were added to 20 mL germanium(IV) chloride ($GeCl_4$, Chengdu Huaxia, 99.99%) ethanol solution (0.05 M) and ultrasonication for 0.5 h, forming a mixed solution and refluxed at 110 ^oC under stirring. Subsequently, 5 mL sodium borohydride ($NaBH_4$,

Aladdin, 98%) ethanol solution (0.69 M) was added to the solution, and then reacted for approximately 10 h. Finally, the black target product Ge-N/O-CNCs were centrifuged, washed thoroughly with ethanol as well as water, and dried. Ge was prepared under the same synthesis process, and only no N/O-CNCs were added. The fabrication process of the Ge-N/O-CNCs is schematically illustrated in Scheme 1.

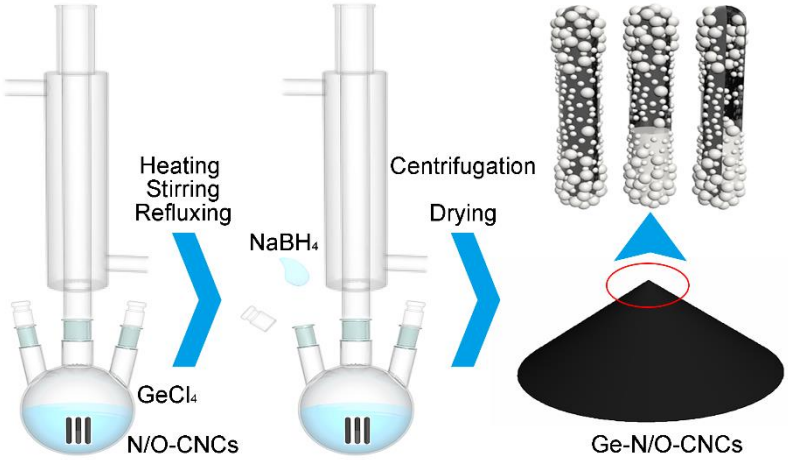

Scheme 1. Schematic demonstration showing the fabrication process of the Ge-N/O-CNCs

2.2 Materials characterizations

The powder X-ray diffraction (XRD) of the resultant materials was characterized on a Philips X-ray diffractometer. The Raman spectroscopy measurements were analysed on a Renishaw in Via Qontor spectrometer. Thermal gravimetric analysis (TGA) was calculated on a METTLER TOLEDO TGA/DSC3+ from 32 ^{o}C to 800 ^{o}C (10 ^{o}C min^{-1}) in the air. X-ray photoelectron spectroscopy (XPS) was performed on an ESCALAB 250Xi spectrometer. The micromorphology of the samples was appeared by the scanning electron microscopy (SEM) on a Hitachi SU-8010. In addition, the moremicromorphology was further analysed by the transmission electron microscopy (TEM) on a Talos F200x instrument.

2.3 Electrochemical analyses

The electrode used for the electrochemical test was made up of active material, polyvinylidene fluoride and acetylene black (mass ratio of 80:10:10). In addition, the cells for testing were fabricated in a glove box filled with argon atmosphere. In the cells, lithium sheet was used as the anode, the prepared electrode was used as the cathode, Celgard 2600 was used as the separator, and 1 M $LiPF_6$ was used as the electrolyte, respectively. The charge-discharge performance measurements of the cell were analysed on a Neware CT-3008 battery cycler (Guangdong, China), and the test range was from 0.01 V to 3.0 V (*vs.* Li/Li^{+}). The electrochemical impedance spectroscopy (EIS) performance measurements of the cell were analysed on a Chenghua CH1660D workstation (Shanghai, China), with a frequency range of 0.01 Hz to 100 kHz for a 5 mV sine wave.

3. RESULTS AND DISCUSSION

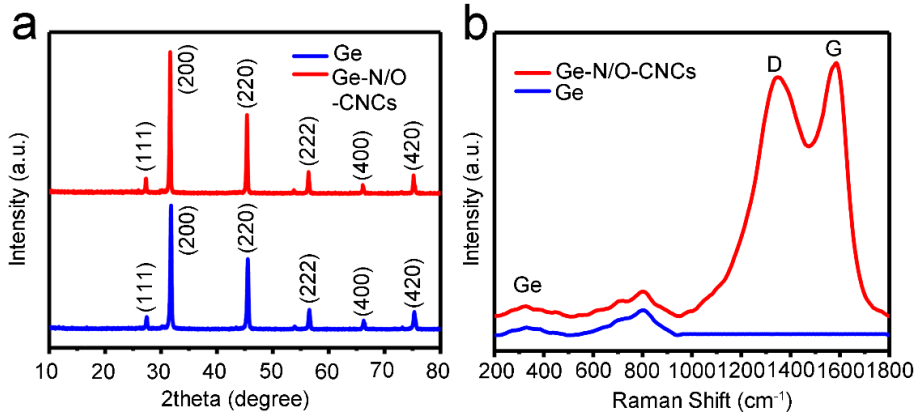

Figure 1. (a) XRD patterns of bare Ge and the Ge-N/O-CNCs. (b) Raman spectra of the Ge-N/O-CNCs and bara Ge.

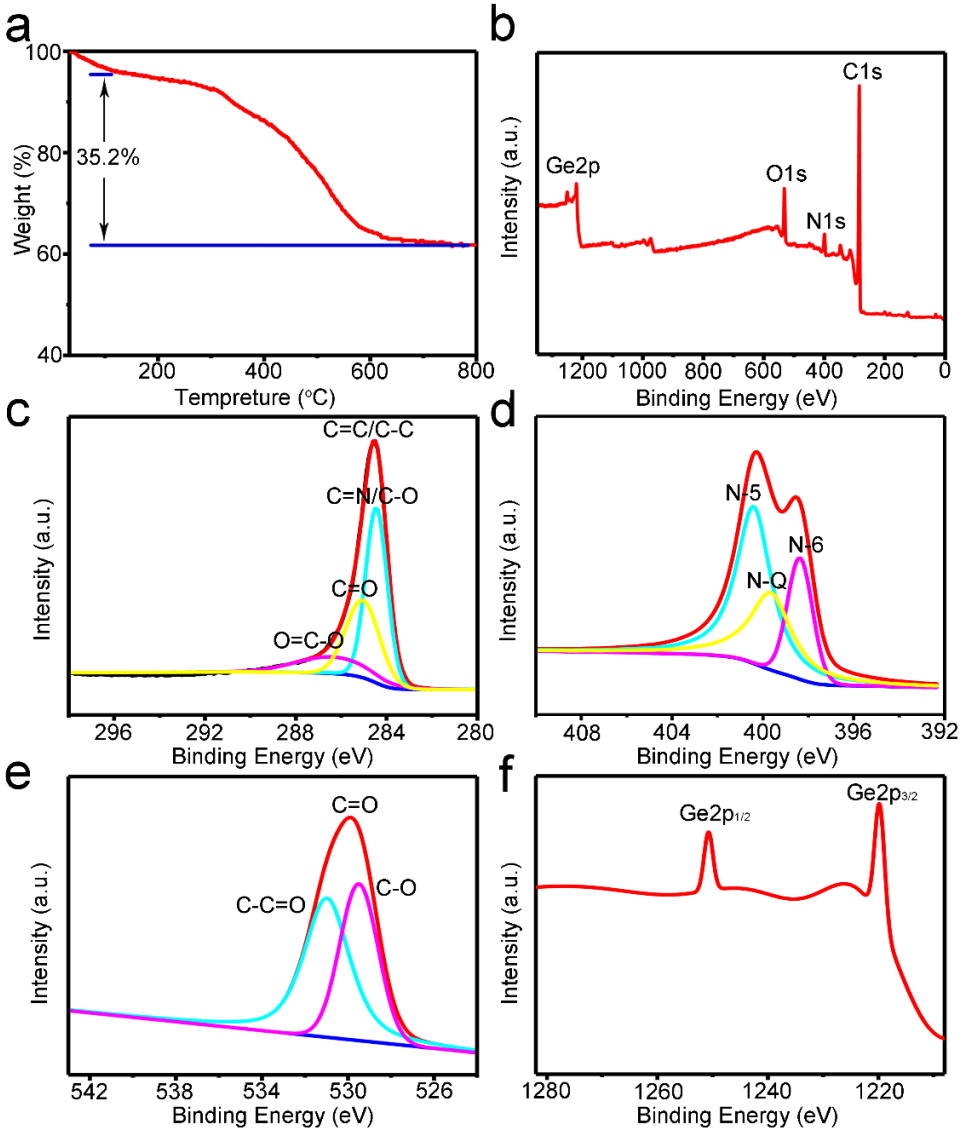

Figure 2. (a) TGA curve of Ge-N/O-CNCs. (b) XPS survey scan spectrum and core level spectrum of (c) C 1s, (d) N 1s, (e) O 1s, and (f) Ge 2p for Ge-N/O-CNCs.

The XRD patterns of bare Ge and Ge-N/O-CNCs are shown in Fig. 1a. It is obvious that all of the characteristic diffraction peaks corresponded to the hexagonal Ge structure (JCPDS No.03-065-9209) [21]. The diffraction peak of N/O-CNCs in the Ge-N/O-CNCs sample was not observed. However, the existence of N-O-CNCs in the Ge-N/O-CNCs sample was confirmed by the Raman spectroscopy (Fig. 1b). Compared to bare Ge, the Raman spectra of Ge-N/O-CNCs contained peaks at ~1357 and 1593 cm^{-1}, which matched the graphene bands D and G. [20,22]

The TGA curves of Ge-N/O-CNCs is shown in Fig. 2a. For Ge-N/O-CNCs, the first weight loss (~3.6 %) is attributed to water evaporation in the temperature range of 32 ^{o}C to 110 ^{o}C. During heating to 800 ^{o}C in the air, according to the reaction Equation (1) and (2), the carbon was oxidized with a loss weight losing its weight in the form of CO_2, as well as Ge was also oxidized to GeO_2 and increased its weight. In summary, the Ge content in the Ge-N/O-CNCs sample can be calculated as ~44.1 %, based on the Equation (3). [22-26]

$$C + O_2 \rightarrow CO_2 \quad \uparrow \qquad (1)$$

$$Ge + O_2 \rightarrow GeO_2 \quad \downarrow \qquad (2)$$

$$Ge\ (wt\ \%) = \frac{\text{atomic mass of Ge}}{\text{molecular mass of GeO2}} \times \frac{\text{weight of the final product}}{\text{initial weight of Ge-N/O-CNCs}} \qquad (3)$$

The elemental composition of the Ge-N/O-CNCs was examined by XPS. The XPS result (Fig. 2b) shows the presence of C, O, and N as well as Ge elements in the sample. Furthermore, the C 1s peak is shown in Fig. 2c and can be separated into O=C-O (~286 eV), C=O (~285 eV), C=C/C-C (~284.6 eV) and C=N/C-O (~284.3 eV), respectively. The N 1s peak is shown in Fig. 2d and can be divided into N-6 (~398 eV), N-Q (~400 eV) and N-5 (~400.5 eV). The peak of O 1s is shown in Fig. 2e and can be divided into C-O (~529.5 eV), C-C=O (~531 eV) as well as C=O (~530 eV). [20] The peaks of Ge 2p are exhibited in Fig. 2f, as the peaks at ~1217 eV and 1250 eV correspond to both the Ge $2p_{3/2}$ and Ge $2p_{1/2}$, indicating that Ge is present in the Ge-N/O-CNCs sample. [18,27]

The SEM image (Fig. 3a) shows that N/O-CNC has a smooth surface. However, the Ge-N/O-CNC has a rough surface, because of the deposition of Ge nanoparticles on the N/O-CNCs matrix. Some broken tubes with holes on the end display the presence of the hollow interior of N/O-CNCs. The TEM image (Fig. 3c) also shows a hollow structure with a rough surface. The HRTEM image (Fig. 3d) shows that the interplanar spacings (0.283 nm, 0.327 nm) correspond to the planes ((200), (111)) of Ge (JCPDS No.03-065-9209) [21]. EDS element mappings are shown in Fig. 4e, which reveals that C, N, and O are homogeneously and regularly distributed around the entire nanocapsule and that Ge is randomly distributed around it.

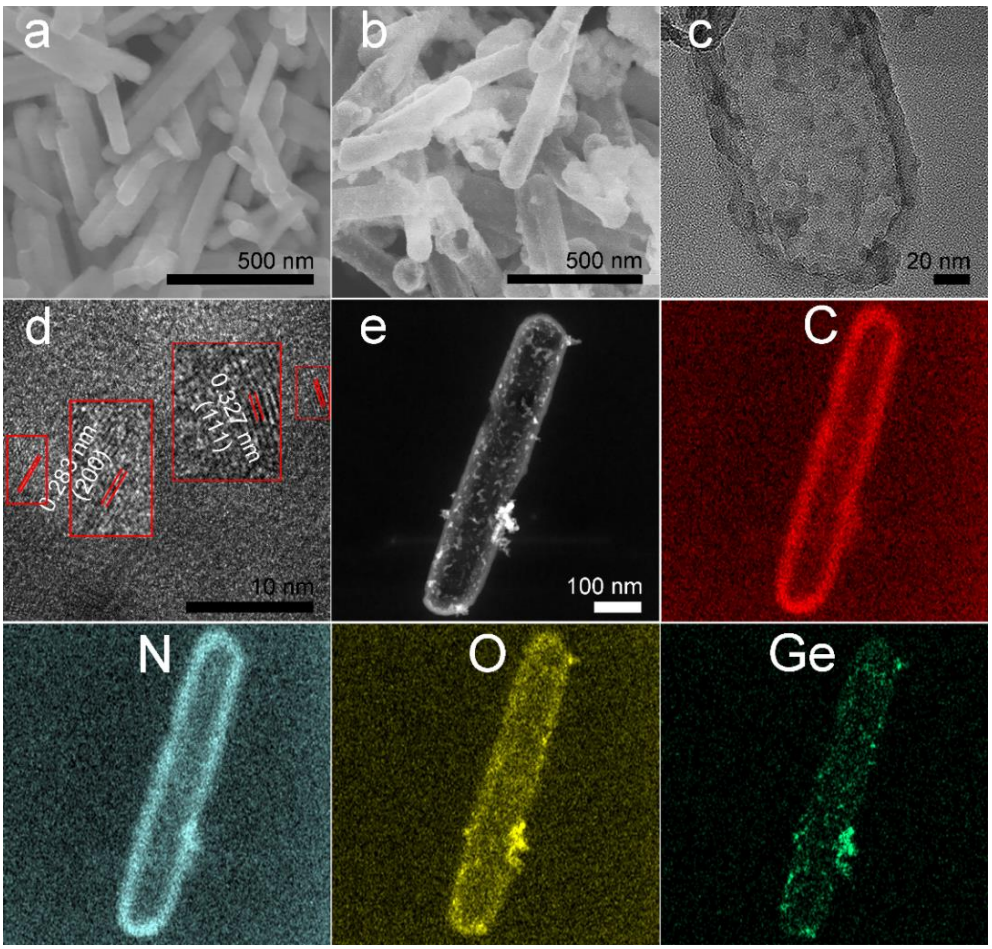

Figure 3. SEM images of (a) N/O-CNCs; (b) Ge-N/O-CNCs. (c)(d) TEM and HRTEM lattice images of Ge-N/O-CNCs, (e) EDS elemental mappings of C, N, O and Ge.

The charge-discharge curves of the Ge-N/O-CNCs and bare Ge electrodes are shown in Fig. 4 (a, b), respectively. Both the first charge capacity and discharge capacity of the Ge-N/O-CNCs electrode are 684 mAh g^{-1} and 1176 mAh g^{-1}, respectively. Simultaneously, the initial coulombic efficiency (CE) of the Ge-N/O-CNCs electrode is 58 %. Compared with the initial CE of bara Ge (44%, Fig. 4b), the initial CE (58 %) of the Ge-N/O-CNCs is significantly higher. The cycling performances of the Ge-N/O-CNCs as well as bare Ge electrodes at a constant current density of 1 A g^{-1} are shown in Fig. 4c. The Ge-N/O-CNCs nanocomposite electrode obtains a high as well as reversible specific capacity of 448 mAh g^{-1} after 100 cycles. However, the bare Ge electrode only gains a low capacity of 127 mAh g^{-1} up to 100 cycles. Apparently, compared to bara Ge, the performance of the Ge-N/O-CNCs electrode was optimized. The rate performance of the Ge-N/O-CNCs electrode was also been investigated (Fig. 4d). The Ge-N/O-CNCs nanocomposite electrode obtains a high as well as reversible specific capacity of 1156 mAh g^{-1} after 10 cycles at 0.16 A g^{-1}. In addition, even if the current density is increased to 3.2 A g^{-1}, it still maintains a capacity of 350 mAh g^{-1}. Moreover, while returning to the initial current density (0.16 A g^{-1}), its capacity recovers back again. In addition, a comparison between Ge/C composites and the previously reported results is displayed in Fig. 4e (detailed parameters are provided in Table 1) [1,15,16,18,22,26-29]. Obviously, the cycling performance of the Ge-N/O-CNCs electrode, which is especially high at a current density, is superior to those reported for Ge/C materials. To characterize the

electrochemical reaction kinetics of the Ge-N/O-CNCs material, EIS measurements were conducted, as shown in Fig. 4f (detailed parameters are provided in Table 2). The semicircle diameter of the Ge-N/O-CNCs electrode was drastically smaller than that of the bara Ge electrode, showing much lower impedance than that of the bare electrode. The low impedance for the Ge-N/O-CNCs benefits from the efficient combination of Ge and N/O-CNCs. EIS results indicated that N/O-CNCs could significantly enhance the electrical conductivity of the composite electrode, which resulted in an appreciable increase in electrochemical reaction kinetics [30,31].

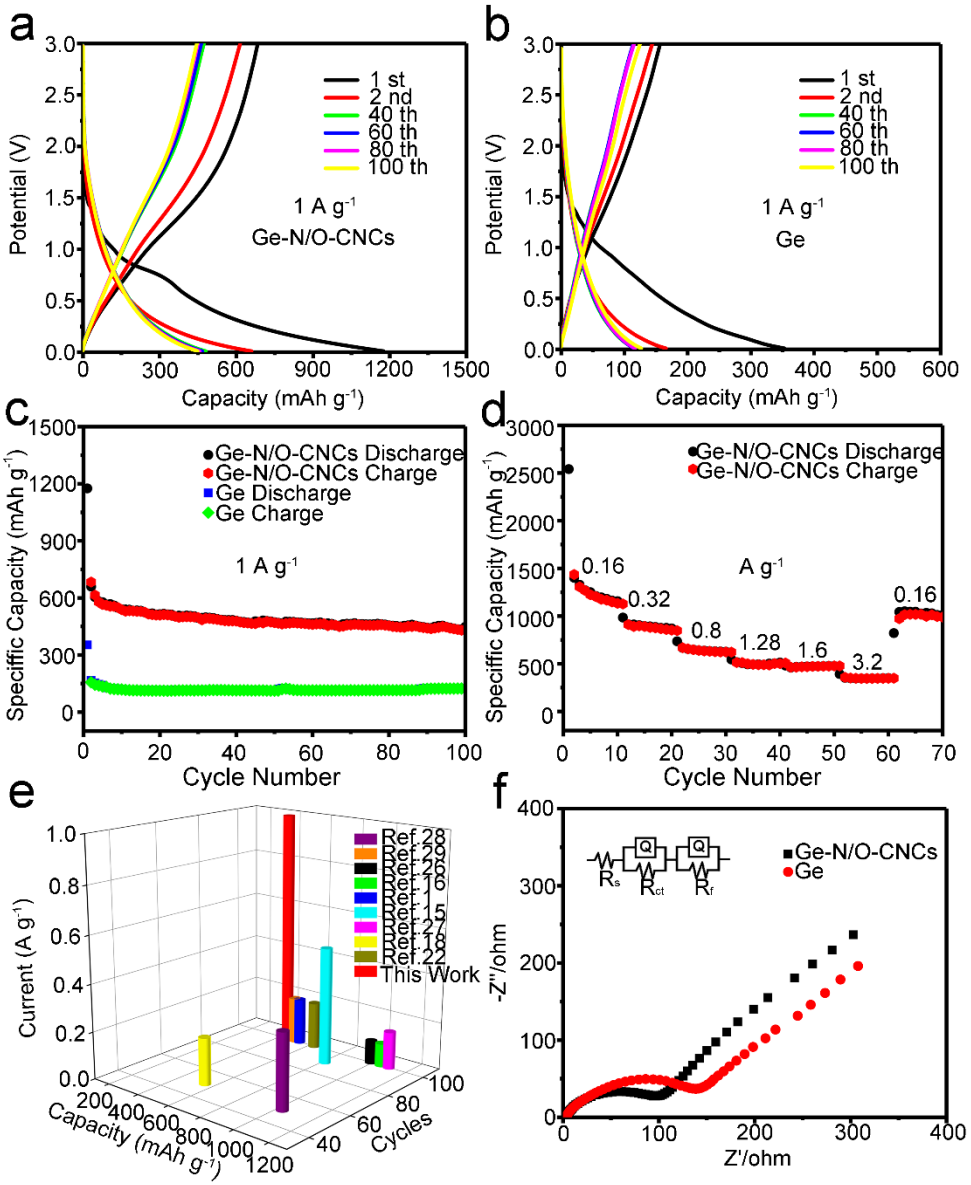

Figure 4. Electrochemical performances of two electrodes: (a, b) Representative charge-discharge profiles of the Ge-N/O-CNCs and the bare Ge, separately. (c) Cycling performance of Ge-N/O-CNCs as well as bare Ge electrodes. (d) Rate performance of Ge-N/O-CNCs electrode. (e) A comparison between Ge/C composites and the previously reported results. (f) EIS of two electrodes after 100 cycles.

Table 1. A comparison between Ge/C composites and the previously reported results

Samples	Cycling Performance			Ref
	Capacity (mA h g^{-1})	Current (A g^{-1})	Cycles	
Ge-C	530	0.2	100	1
Ge@C-N	813	0.5	90	15
Ge@G@TiO_2 NFs	1050	0.1	100	16
Ge@CNF@C	550	0.2	50	18
Ge-C	627	0.2	100	22
Ge/C	496	0.2	100	26
3D-Void/Ge@C	990	0.1	100	27
Ge/PPY	1029	0.32	50	28
Ge@C sphere	1099	0.16	100	29
Ge-N/O-CNCs	448	1	100	our work

Table 2. EIS of Ge-N/O-CNCs and bare Ge electrodes after 100 cycles

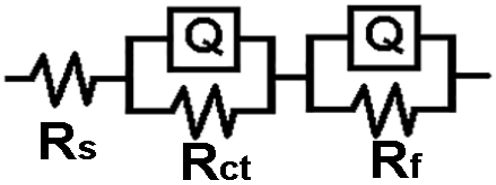

Samples	R_s(Ω)	R_{ct}(Ω)	R_f(Ω)
Ge-N/O-CNCs	3.299	91.47	930
Ge	2.844	128.7	1912

4. CONCLUSIONS

In summary, we designed and synthesized of a novel Ge-N/O-CNCs nanoarchitecture via a simple heating reflux method. The Ge nanoparticles are distributed in the hollow carbon nanocapsule can not only prevent aggregation of Ge nanoparticles but also facilitate the rapid transport of electrons. The Ge-N/O-CNCs electrode showed a discharge capacity of 448 mAh g^{-1} after 100 cycles at 1 A g^{-1}. It still had a specific capacity of 350 mAh g^{-1} even at a high rate of 3.2 A g^{-1}. When returned to 0.16 A g^{-1}, its specific capacity quickly recovered to 1011 mAh g^{-1}. When LIBs anodes were used, they exhibited high electrochemical performance.

ACKNOWLEDGEMENTS
This work is supported by the National Natural Science Foundation of China (Nos: 21601122) and the Belt and Road Initiatives International Cooperation Project (No. 20640770300).

NOTES
The authors declare no competing financial interest.

References

1. W. Guo, L. Mei, Q. Feng and J. Ma, *Mater. Chem. Phys.*, 168 (2015) 6.
2. Y. Cai, X. Li, L. Wang, H. Y. Gao, Y. N. Zhao and J. M. Ma, *J. Mater. Chem. A*, 3 (2015) 1396.
3. X. Li, J. T. Xu, Z. J. Zhang, L. Mei, C. Y. Cui, H. K. Liu, J. M. Ma and S. X. Dou, *J. Mater. Chem. A*, 3 (2015) 3257.
4. L. Liu, Z. Song, J. Wang, L. Shen, B. Tu, S. Wang and D. Mao, *Int. J. Electrochem. Sci.*, 11 (2016) 8654.
5. D. M. Kim, Y. W. Lee, S. J. Kim, M. C. Kim, G. H. Lee, H. S. Choe, W. Huh and K. W. Park, *Int. J. Electrochem. Sci.*, 11 (2016) 3591.
6. T. Song, Y. Jeon, M. Samal, H. Han, H. Park, J. Ha, D. K. Yi, J. M. Choi, H. Chang, Y. M. Choi and U. Paik, *Energy Environ. Sci.*, 5 (2012) 9028.
7. K.Edström, M. Herstedt and D. P. Abraham, *J. Power Sources*, 153 (2006) 380.
8. L. C. Yang, Q. S. Gao, L. Li, Y. Tang and Y. P. Wu, *Electrochem. Commun*, 12 (2010) 418.
9. H. Wu, G. Chan, J. W. Choi, I. Ryu, Y. Yao, M. T. McDowell, S. W. Lee, A. Jackson, Y. Yang, L. Hu and Y. Cui, *Nat. Nanotechnol.*, 7 (2012) 310.
10. G. Cui, L. Gu, L. Zhi, N, Kaskhedikar, P. A. Aken, K. Müllen and J. Mainer, *Adv. Mater.*, 20 (2008) 3079.
11. M. H. Park, Y. H. Cho, K. Kim, J. Kim, M. Liu and J. Cho, *Angew. Chem. Int. Ed.*, 41 (2011) 9647.
12. M. H. Seo, M. Park, K. T. Lee, K. Kim, J. Kim and J. Cho, *Energy Environ. Sci.*, 4 (2011) 425.
13. J. Liu, K. Song, C. Zhu, C. C. Chen, P. A. Aken, J. Maier and Y. Yu, *ACS Nano*, 8 (2014) 7051.
14. C. Yao, J. Wang, H. Bao and Y. Shi, *Mater. Lett.*, 124 (2014) 73.
15. Y. Xiao and M. Cao, *ACS Appl. Mater. Interfaces*, 6 (2014) 12922.
16. X. Wang, L. Fan, D. Gong, J. Zhu, Q. Zhang, B. Lu, *Adv. Funct. Mater.*, 26.7 (2016) 1104.
17. W. Li, Z. Jie, T. Chen, W. Teng, X. Wang and X. Li, *Chem. Commun.*, 45 (2014) 2052.
18. S. Li, C. Chen, K. Fu, R. White, C. Zhao, P. D. Bradford and X. Zhang, *J. Power Sources*, 253 (2014) 366.
19. D. H. Youn, N. A. Patterson, H. Park, A. Heller and C. B. Mullins, *ACS Appl. Mater. Interfaces*, 8 (2016) 27788.
20. L. Wang, B. Lu, S. Wang, W. Cheng, Y. Zhao, J. Zhang and X. Sun, *J. Mater. Chem. A*, 7 (2019) 11117.
21. W. Witt, Z. *Naturforschg. A*, 22 (1967) 92.
22. H. Choe, S. Kim, M. Kim, D. Kim, G. Lee, S. Han, D. Kwak and K. Park, *RSC Adv.*, 6 (2016) 72926.
23. Y. Xu, X. Zhu, X. Zhou, X. Liu, Y. Liu, Z. Dai and J. Bao, *J. Phys. Chem. C* , 118 (2014) 28502.
24. L. Zhao, L. Wang, S. Zeng, Q. Liu, W. Yan, M. Liu, H. Gong and J. Zhang, *J. Mater. Sci.*, 55 (2020) 14491.
25. L. Han, J. Tang, R. Yang, Q. Wei and M. Wei, *Nano*, 13 (2021) 5307.
26. Y. W. Lee, D. M. Kim, S. J. Kim, H. S. Chae, K. H. Lee, J. I. Sohn, S. N. Cha, J. M. Kim and K. W. Park, *ACS Appl. Mater. Interfaces*, 11 (2016) 7022.
27. X. Liu, T. Ji, T. Nie, T. Wang, Z. Liu, S. Liu, J. Zhao and Y. Li, *Mater. Lett.*, 261 (2019) 127157.
28. X. Gao, W. Luo, C. Zhong, D. Wexler, S. L. Chou, H. K. Liu, Z. Shi, G. Chen, K. Ozawa, J. Z.

Wang, *Rep*., 4 (2014) 6095.
29. M. Liu, X. Ma, L. Gan L, D. Zhu and L. Chen, *J. Mater. Chem. A*, 2 (2014) 17107.
30. M. W. Forney, M. J. Dzara, A. L. Doucett, M. J. Ganter, J. W. Staub, R. D. Ridgley and B. J. Landi, *J. Mater. Chem. A*, 2.35 (2014) 14528.
31. P. Kitschke, M. Walter, T. Rueffer, H. Lang, M. V. Kovalenko and M. Mehring, *J. Mater. Chem. A*, 45 (2016) 5741.